Behavior of steel columns with double curvature: a numerical simulation and design-oriented parametric study

Hamda Guedaoura
Faculty of Sciences and Technology, Department of Civil Engineering, Chadli Bendjedid-El Tarf University, P. O. Box 73, 36000 El Tarf, Algeria
Materials Geomaterials and Environment Laboratory (LMGE), Faculty of Technology, Department of Civil Engineering, Badji Mokhtar-Annaba University, P.O. Box 12, Annaba 23000, Algeria
h.guedaoura@univ-eltarf.dz, https://orcid.org/0009-0002-7988-893X

Mohammed Benzerara
Materials Geomaterials and Environment Laboratory (LMGE), Faculty of Technology, Department of Civil Engineering, Badji Mokhtar-Annaba University, P.O. Box 12, Annaba 23000, Algeria
mohammed.benzerara@univ-annaba.dz, https://orcid.org/0009-0000-0633-1140

Nadia Gouider, Yazid Hadidane
Civil Engineering Laboratory, Faculty of Technology, Department of Civil Engineering, Badji Mokhtar-Annaba University, P.O. Box 12, Annaba 23000, Algeria
nadia.gouider@univ-annaba.dz, https://orcid.org/0009-0003-7420-2983
yazid.hadidane@univ-annaba.dz, https://orcid.org/0009-0001-4324-609X

Anfel Chaima Hadidane
Civil Engineering Department, Istanbul Gelisim University, Avcilar, Turkey
anfel.hadidane@ogr.gelisim.edu.tr, https://orcid.org/0009-0001-3366-5979

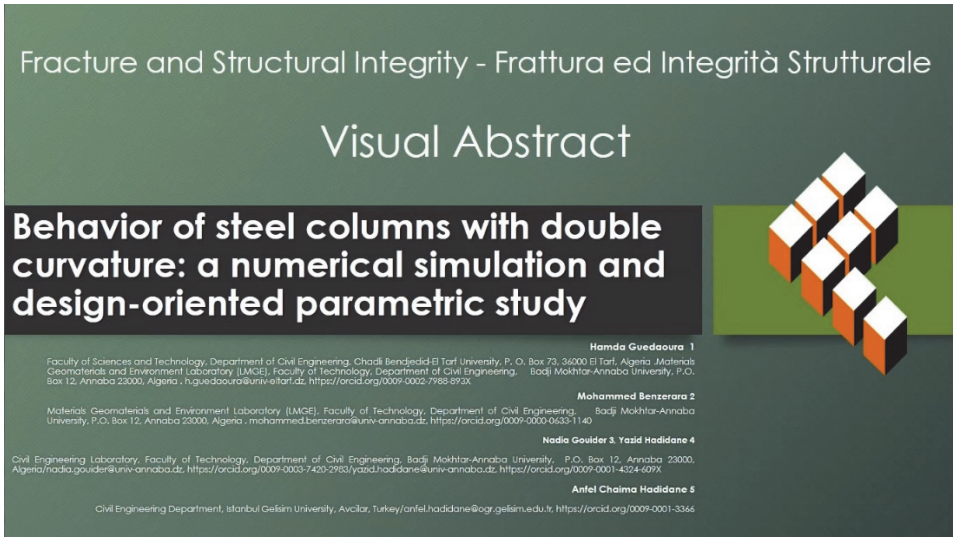

Citation: Guedaoura, H., Benzerara, M., Guider, N., Hadidane, Y., Hadidane, A. C., , Behavior of steel columns with double curvature: a numerical simulation and design-oriented parametric study, Fracture and Structural Integrity, 74 (2025) 171-192.

Received: 12.06.2025
Accepted: 25.08.2025
Published: 26.08.2025
Issue: 10.2025

KEYWORDS. Steel columns, Double curved columns, Axial load capacity, Failure mechanisms, Experimental analysis, Modeling.

INTRODUCTION

Over the past few decades, architectural trends have increasingly favored expressive and fluid forms, moving away from rigid, rectilinear geometries. This evolution has been facilitated by advances in digital design tools and construction technologies, enabling architects to explore complex spatial configurations that were once impractical or impossible to realize. Among these transformations, the emergence of curved structural elements particularly non-linear columns has become a defining feature of contemporary design language. Curved columns are no longer viewed merely as support elements but are now often used to convey motion, rhythm, and continuity within a space. As highlighted by Hengsheng [1] in his study, curvature in modern architecture enhances not only the structural behavior through efficient load distribution but also the user's spatial perception and the building's environmental integration.

The inclusion of curved or double-curved columns introduces significant challenges from a structural engineering standpoint (Fig. 1). Unlike traditional prismatic members, curved columns exhibit complex load paths and demand more sophisticated analysis techniques to capture their nonlinear response under axial and lateral forces. Standard design codes offer limited guidance for these geometries, prompting the need for customized modeling approaches.

Figure 1: Architectural trends using curved columns [2].

In recent years, significant research has explored the structural behavior of hollow steel columns. Sediek et al. [3] conducted detailed finite-element simulations on HSS columns subjected to axial and lateral forces, highlighting the influence of local, global slenderness and initial axial load effect on collapse behavior . Similarly, Hilo et al. [4] conducted an extensive parametric study on polygonal hollow steel columns with various cross-sectional shapes, using eighty finite element models to investigate their axial load behavior. Their findings revealed that the shape of the cross-section significantly influences the axial resistance, with rectangular profiles exhibiting higher load-bearing capacity compared to circular or oval ones.

Lin-Hai Han et al. [5] carried out a series of experimental investigations on 18 curved concrete-filled steel tubular (CCFST) members with both circular and square cross-sections under axial compression. The study aimed to assess the impact of initial geometric imperfections and slenderness on the structural behavior of these elements, and to compare their performance with that of conventional straight CFST columns subjected to eccentric loading but without initial curvature. The findings revealed that the curved members exhibited notably ductile responses, and their load-bearing capacities were slightly enhanced compared to their straight counterparts. Moreover, the numerical approach developed in the study demonstrated good correlation with the experimental outcomes. In a subsequent study, the same research team investigated the behavior of 20 curved concrete-filled steel tubular (CCFST) specimens[6]. Zheng et al. [7] experimentally investigated

the compressive behavior of circular curved concrete-filled stainless steel tubular (CCFSST) struts. Their results showed that CCFSST members exhibited global buckling failure, and under concentric loading, their axial capacity slightly exceeded that of equivalent straight CFSST columns, with differences within 5%. This work focused on examining the effects of key parameters such as: the initial curvature ratio, nominal slenderness ratio and the configuration of bracing systems. It was found that both the load-carrying capacity and overall stiffness of the built-up CCFST specimens were observed to diminish as the initial curvature ratio or the nominal slenderness increased. Besides that the inclusion of concrete within the chord tubes significantly enhances the structural performance of curved built-up members.

Yiğit ERKOÇ et al. [8] indicated that enlarging the cross-sectional dimensions of inclined columns leads to a reduction in the effective usable floor area, while also driving up construction costs due to the increased consumption of concrete and steel particularly in innovative twisted architectural designs. Conventionally, columns featuring curved, twisted, or otherwise unconventional geometries have been regarded primarily as architectural elements, with limited structural contribution or load-bearing functionality. However, recent studies have begun to challenge this perception, demonstrating that such geometrically complex columns can indeed possess significant structural potential. Emerging evidence highlights their effectiveness not only in carrying axial or lateral loads but also in enhancing seismic performance when integrated into structural systems, either as primary elements or as part of advanced retrofitting strategies. Kun-Sian Lin et al. [9] proposed retrofitting strategy using curved column members to enhance seismic performance. The results indicated that the retrofitted column bases exhibited improved ductility, primarily due to the expansion of the plastic zone. This enhancement was attributed to the early yielding of the curved member and the delayed yielding of the anchor rods at the original column interface. Pi and Bradford [10] found that contrary to common assumptions, prebuckling deformations may reduce the buckling moment in laterally fixed arches under positive bending and only increase it under negative bending when the included angle is large. In structure's applications, it is impossible to achieve pure axial compression without accompanying moments, as factors such as structural imperfections, eccentricities, displacement of supports, and uneven loading inevitably introduce additional forces. Pi and Trahair [11] investigated the in-plane elastic buckling of circular arches, taking into account the influence of boundary conditions, including angle, and loading position. Their study emphasized that arches with larger included angles and pinned ends are more prone to buckling, especially when subjected to central loading. Vertically curved components in structures are subjected to both axial compression and bending forces within the plane[12]. The mechanical response of curved steel columns has attracted attention in recent years due to their architectural appeal and structural complexity. While several studies have addressed straight or prismatic members under compression, limited research is available on the nonlinear behavior of curved elements. Jolly Monge [13] demonstrated the feasibility of casting double-curved reinforced concrete columns using flexible formworks, achieving organic shapes with minimal construction complexity and improved spatial quality. This architectural innovation, realized through full-scale in-situ experimentation, opens new pathways for integrating form and function in vertical load-bearing elements. While such studies emphasize the expressive potential of concrete, the structural implications of these complex geometries remain largely under-investigated especially for hollow steel. Pi and Bradford [14] investigated the inelastic flexural–torsional buckling behavior and strength of steel I-section arches with central elastic torsional restraints. Their study demonstrated that such restraints can enhance the structural capacity, although the effectiveness diminishes with decreasing slenderness. While their research focused on curved arches, the influence of torsional restraints and slenderness effects provides useful insight into the stability behavior of other curved members. Wei et al. [15] investigated the in-plane buckling behavior of parabolic fixed steel arches using a nonlinear finite element approach, highlighting the strong influence of rise-to-span ratio and initial imperfections on critical loads. Although their work focused on arch-type structures, the proposed equivalent beam-column method and their treatment of geometric nonlinearity offer valuable insights applicable to the stability analysis of double-curved steel columns, particularly in how curvature modifies global and local instability patterns. Mohammed et al. [16] investigated the behavior of geometrically nonlinear steel columns through a validated finite element model, focusing on variations in column length, included angle, and boundary conditions. Their results demonstrated that such nonlinear columns exhibit responses similar to arches up to the buckling point, highlighting the significant influence of geometric nonlinearity. Moreover, their work revealed a noticeable gap in current design codes regarding the treatment of these structural elements, reinforcing the need for further research in this domain.

Khalkhali et al. [17] have provided valuable insights into the behavior of double-curved square tubes under quasi-static axial compression, employing a comprehensive experimental and numerical approach. Their work successfully characterized the plastic deformation mechanisms and the energy absorption potential of these curved members, while also elucidating the influence of geometric variables on global folding modes. This study serves as a robust framework for understanding the crushing behavior of small scale double curved structural profiles.

Building on this foundation, the present research explores hollow steel columns with double curvature, introducing alternative geometric configurations and curvature parameters to assess their impact on load-bearing performance. Despite

significant advances in structural engineering, the load-bearing capacity of metal columns with double-curved profiles remains largely unexplored, as most existing research focuses on straight or mildly curved columns with infilled concrete. This first in-depth study on the load-bearing capacities, failure modes, and load-displacement behavior of large-scale double-curved hollow steel columns holds significant potential for the development of robust design principles for these elements in modern construction, expanding the design space for non-prismatic elements and offering practical insights for their structural application.

DESCRIPTION AND VALIDATION OF THE FINITE ELEMENT MODEL BASED ON PREVIOUS EXPERIMENTAL STUDIES

Finite element model description

This study develops and validates a comprehensive three-dimensional (3D) finite element model using the commercial finite element software ABAQUS/CAE [18], with the primary objective of investigating the nonlinear response of double-curved hollow steel columns under axial compression. Given the highly nonlinear behavior anticipated in such geometrically complex members including large displacements, progressive local buckling, and post-buckling deformation. Robust numerical framework was required to capture these phenomena accurately while maintaining computational efficiency. For this purpose, the ABAQUS/Explicit solver, originally intended for dynamic simulations, was employed due to its proven capability to effectively handle quasi-static problems involving severe contact interactions, geometric instability, and material nonlinearity, as reported in prior studies [18,19]. Although explicit solvers are typically associated with high-speed dynamic analyses, their application to quasi-static simulations has gained traction, particularly for structural problems characterized by high degrees of nonlinearities where conventional implicit solvers may experience convergence difficulties. However, to ensure that inertial effects remained negligible and the analysis remained within the quasi-static regime, it was crucial to adopt a carefully calibrated simulation strategy. This was initiated by performing a preliminary modal analysis, which served to identify the fundamental natural frequencies of the element. Based on these values, an appropriate total analysis time was selected, long enough to suppress dynamic amplification effects and prevent the introduction of high-frequency oscillations that could distort the physical interpretation of the results. To further reduce dynamic effects, the applied displacement loading was modulated using a smooth step amplitude, allowing for a gradual and continuous increase in the applied load. This approach prevented abrupt force application, which is known to generate excessive kinetic energy and cause stress wave propagation, particularly in thin-walled components [20]. Throughout the analysis, a strict energy monitoring procedure was implemented to validate the quasi-static nature of the solution. Specifically, the ratio of kinetic energy to internal energy was tracked in real time, and efforts were made to ensure that the kinetic energy remained at least an order of magnitude smaller than the internal energy, thus confirming that the response was dominated by structural deformation rather than inertia [18]. This strategy collectively ensured that the use of the explicit solver yielded physically realistic results with high numerical stability, while capturing the complex nonlinear response of the double-curved steel columns with precision. The numerical model was formulated by incorporating both geometric and material nonlinearities to accurately capture the complex structural behavior of double-curved hollow columns. Geometric nonlinearity was introduced to account for second-order effects associated with large displacements and rotations, particularly where axial loading amplifies deformation. Material nonlinearity was included to simulate the inelastic response of steel, encompassing yielding, strain hardening, and plastic redistribution. The combined implementation of these nonlinearities enables a comprehensive and realistic prediction of both global and local responses, with particular emphasis on post-buckling behavior, local instabilities, and progressive strength degradation [20]. The material behavior of the steel employed in the simulation was characterized using an idealized bilinear stress–strain model. This simplified representation enables the accurate capture of elastic–plastic transitions while maintaining computational efficiency. The finite element formulation incorporated four-node doubly curved shell elements (S4R), which are widely recognized for their robustness in handling large displacements and rotations, particularly in geometries involving complex curvature. To ensure reliable through-thickness stress integration and to appropriately capture bending effects and localized instability phenomena, Gauss integration points were employed along the shell thickness. The FE model deliberately excluded the influence of initial geometric imperfections and residual stresses, in accordance with recommendations from prior validated study [21], which demonstrated that these effects exert a limited influence on the global structural response of compact elements with uniform curvature. Regarding mesh sensitivity, a mesh convergence study was conducted, and a uniform mesh size of 40 mm × 40 mm was ultimately adopted. This mesh density offered a balanced compromise between numerical accuracy and computational demand and was shown to yield results in close agreement with available experimental data in terms of initial stiffness, ultimate load capacity, and overall load–displacement behavior. Furthermore, the applied boundary conditions

were rigorously modeled to mirror those implemented in the experimental setup, as shown in Fig. 2, ensuring consistency and enabling meaningful comparative validation. The validation of the proposed finite element model was conducted by systematically comparing its output with experimental findings available in the literature. Given the novelty of the present study, which focuses on the structural behavior of double-curved hollow steel columns, an extensive literature review was performed to identify relevant experimental benchmarks. Among the few studies addressing such geometric configurations, the work carried out by A. Khalkhali et al. [17] was deemed the most suitable reference, as it involved axial compression tests on cold-formed square steel tubes exhibiting intentional double curvature. This experimental investigation served as a basis for assessing the predictive capability of the numerical model, particularly in terms of load-bearing capacity, deformation mode, and post-buckling response. In the referenced study, four specimens with distinct curvature profiles and geometric characteristics—designated A1, A2, A3, and B1—were tested under quasi-static axial loading. These configurations are comprehensively illustrated in Fig. 3 and detailed in Tab. 1. While the curvature and local geometry varied between the specimens, the remaining dimensional parameters were kept constant across all tests, with a uniform total length L=1000 mm and a wall thickness t=2 mm. The experimental setup and loading conditions applied in [17] were meticulously replicated within the numerical framework to ensure the reliability of the comparison.

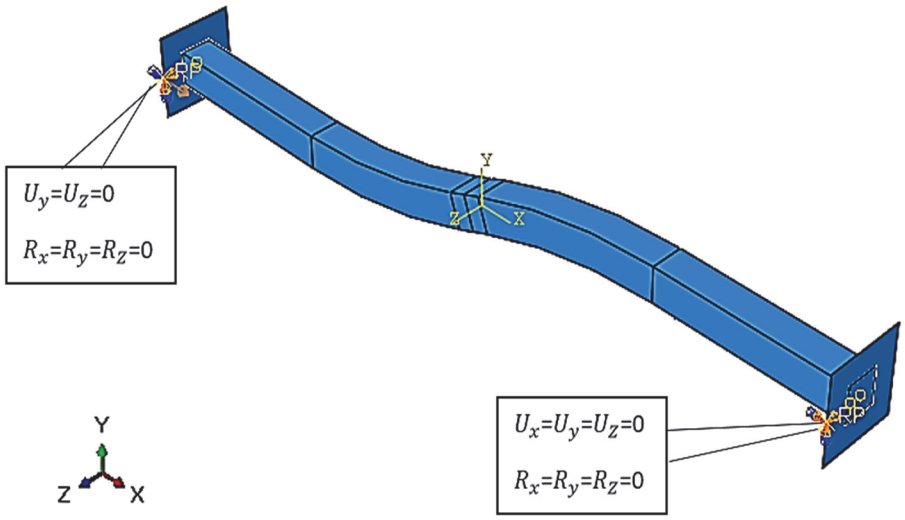

Figure 2: In Boundary conditions of specimen A1 tested by A. Khalkhali et al. [17].

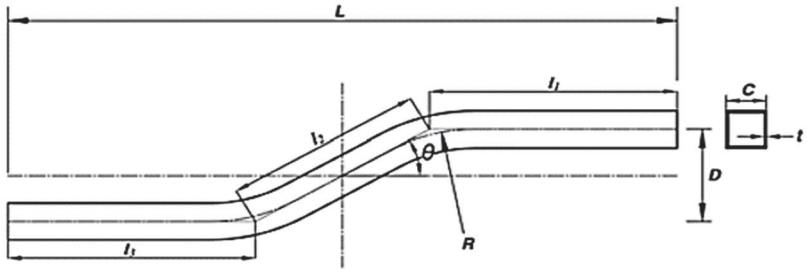

Figure 3: Geometric configuration of the specimen with double curvature tested by A. Khalkhali et al. [17].

Specimen	C (mm)	θ (deg)	R (mm)	D (mm)	f_y (MPa)	E (GPa)
A1	40	20	700	100	200	195
A2	40	20	950	150	200	195
A3	40	30	450	150	200	195
B1	50	20	950	150	200	195

Table 1: Test Specimen Geometry and mechanical properties According to A. Khalkhali et al. [17].

The flat plate, acting as a fixture at both the top and bottom during the experiments, was modeled as a rigid analytical surface. It was allowed to move solely along the x-direction at the top, while all degrees of freedom at the lower end were constrained. The tube was fully connected to the plates through tied constraints. The simulation results were then benchmarked against the experimental data in terms of global load–displacement behavior, ultimate capacity, and observable deformation patterns, offering a comprehensive validation of the modeling approach employed in this study

Figure 4: Initial Shape of specimen A1 Tested by A. Khalkhali et al. [17].

Finite element model validation

Fig. 5 presents a comparative analysis between the numerical simulations and the experimental load–displacement curves. A strong correlation can be observed between both sets of results. Initially, the reaction force rises sharply, indicating an elastic behavior up to the yield point. Once yielding initiates, plastic deformation begins to spread. Following this stage, the reaction force gradually declines as the displacement continues to increase. The ultimate load predicted by the numerical model differs from the experimental results by 11% to 24% as shown in Tab. 2. This indicates a reasonably good agreement considering the complexity of the tested configurations. Furthermore, the overall structural behavior is well captured by the simulation, as evidenced by the close agreement in deformation shapes and failure modes between the numerical and experimental results. It is important also to highlight that geometric imperfections arising from the manufacturing process may lead to a slight decrease in the peak load capacity [17]. Fig. 6 presents the deformed shapes corresponding to the failure modes of specimens A1, A2, A3 and B1 both experimentally and numerically, at a displacement of around 300 mm at the top of the specimens. These figures reveal a high level of correspondence between the experimental results and the numerical simulations; Plastic collapse is expected to initiate at the transition zones where the specimen geometry shifts from a straight to a curved profile. Sudden geometric transitions can lead to localized stress intensification, thereby affecting the overall deformation behavior.

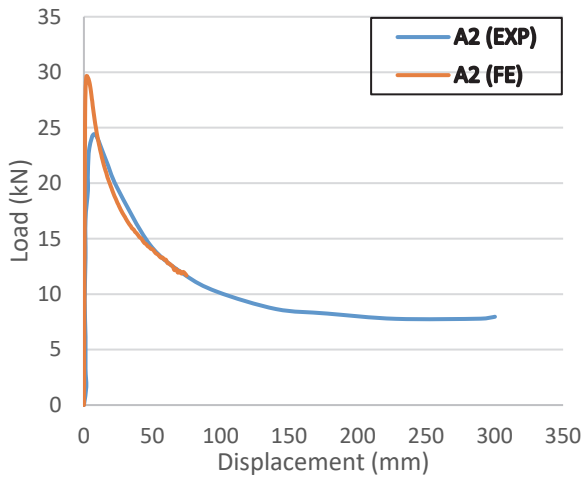

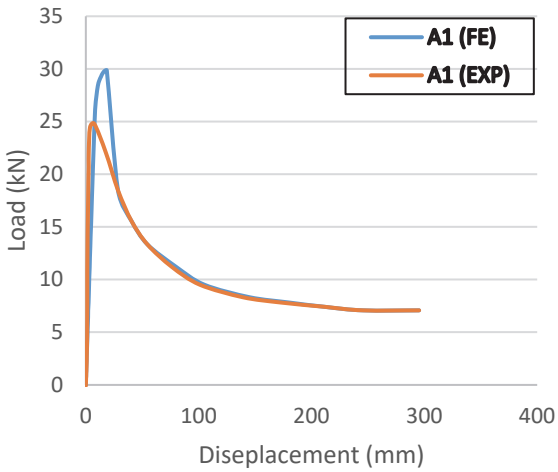

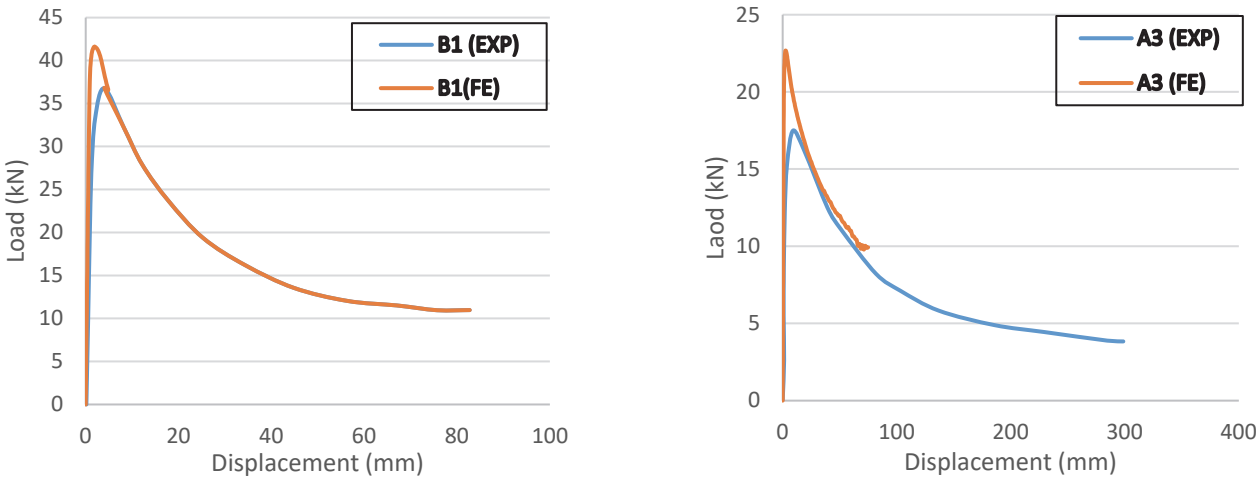

Figure 5: Load-displacement response of tested specimens.

Specimen	Pu EXP (Kn)	Pu FE (Kn)	(Pu EXP)/(Pu FE)
A1	25	29	0,86
A2	24,41	29,24	0,83
A3	17	22,40	0,76
B1	37	41,48	0,89

Table 2: Ultimate load assessment: experimental data compared to FE predictions.

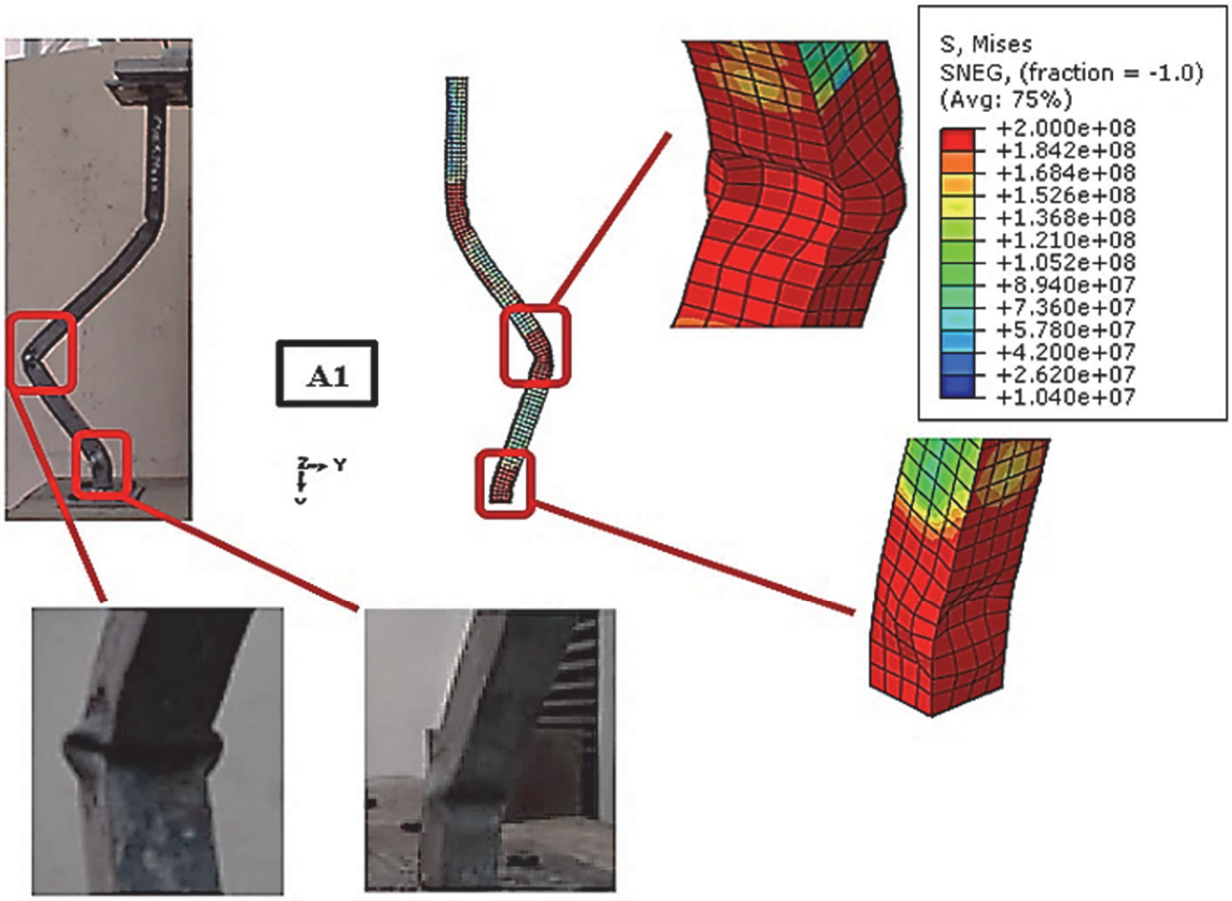

(a)

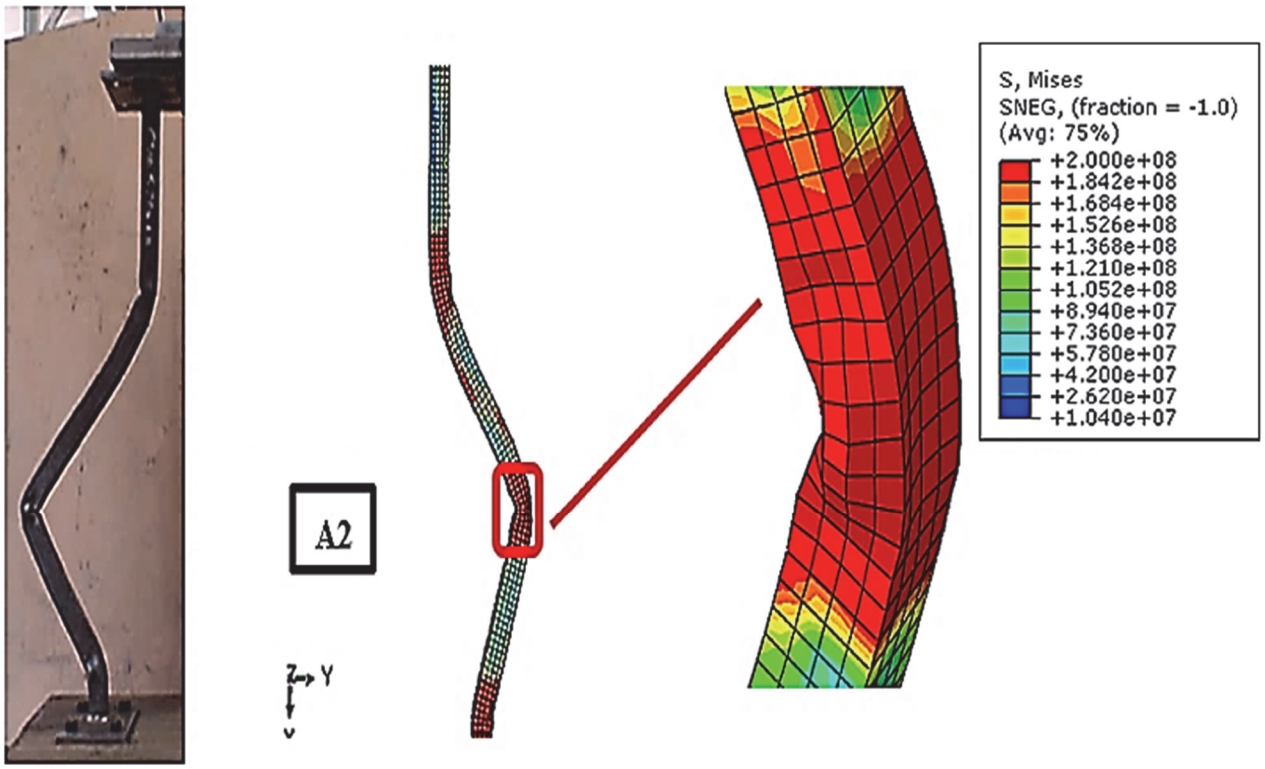
A2
S, Mises
SNEG, (fraction = -1.0)
(Avg: 75%)
+2.000e+08
+1.842e+08
+1.684e+08
+1.526e+08
+1.368e+08
+1.210e+08
+1.052e+08
+8.940e+07
+7.360e+07
+5.780e+07
+4.200e+07
+2.620e+07
+1.040e+07
Y

(b)

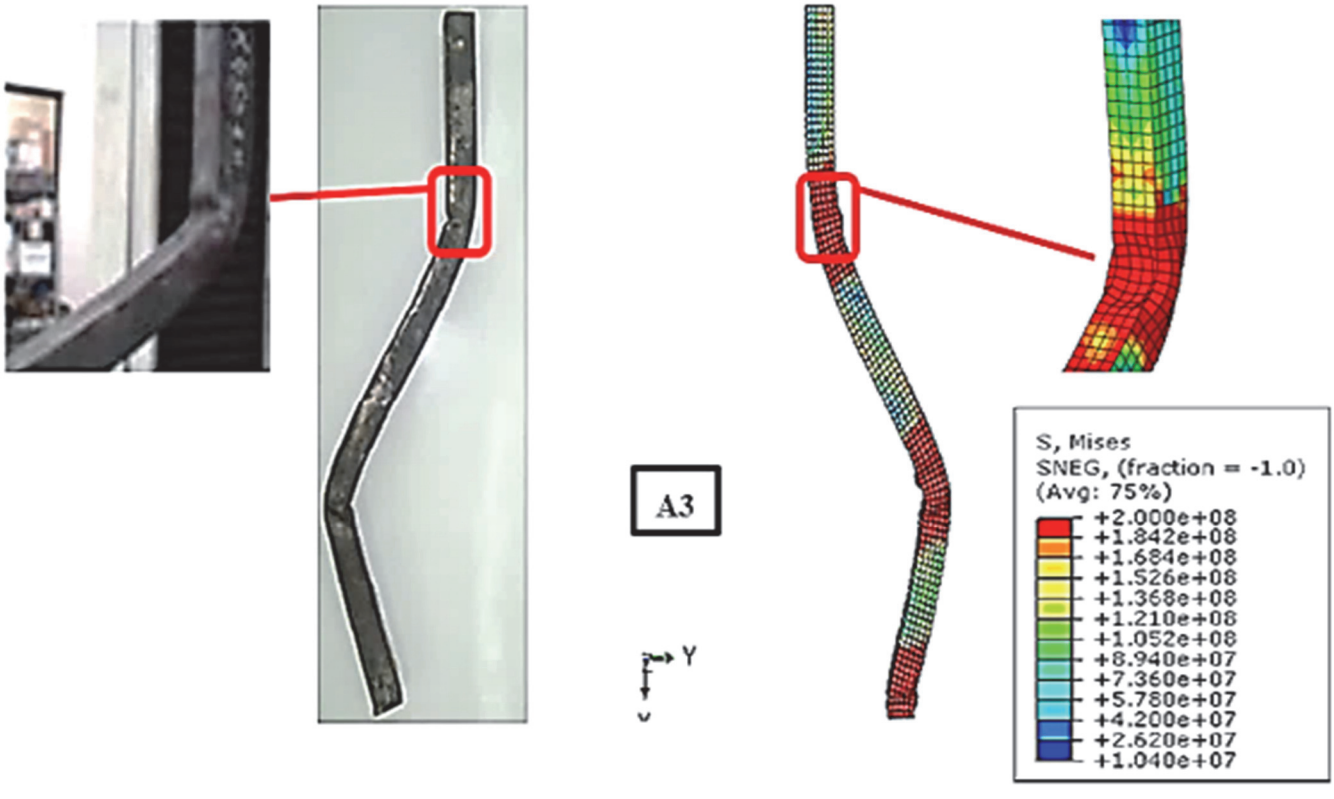
A3
S, Mises
SNEG, (fraction = -1.0)
(Avg: 75%)
+2.000e+08
+1.842e+08
+1.684e+08
+1.526e+08
+1.368e+08
+1.210e+08
+1.052e+08
+8.940e+07
+7.360e+07
+5.780e+07
+4.200e+07
+2.620e+07
+1.040e+07
Y

(c)

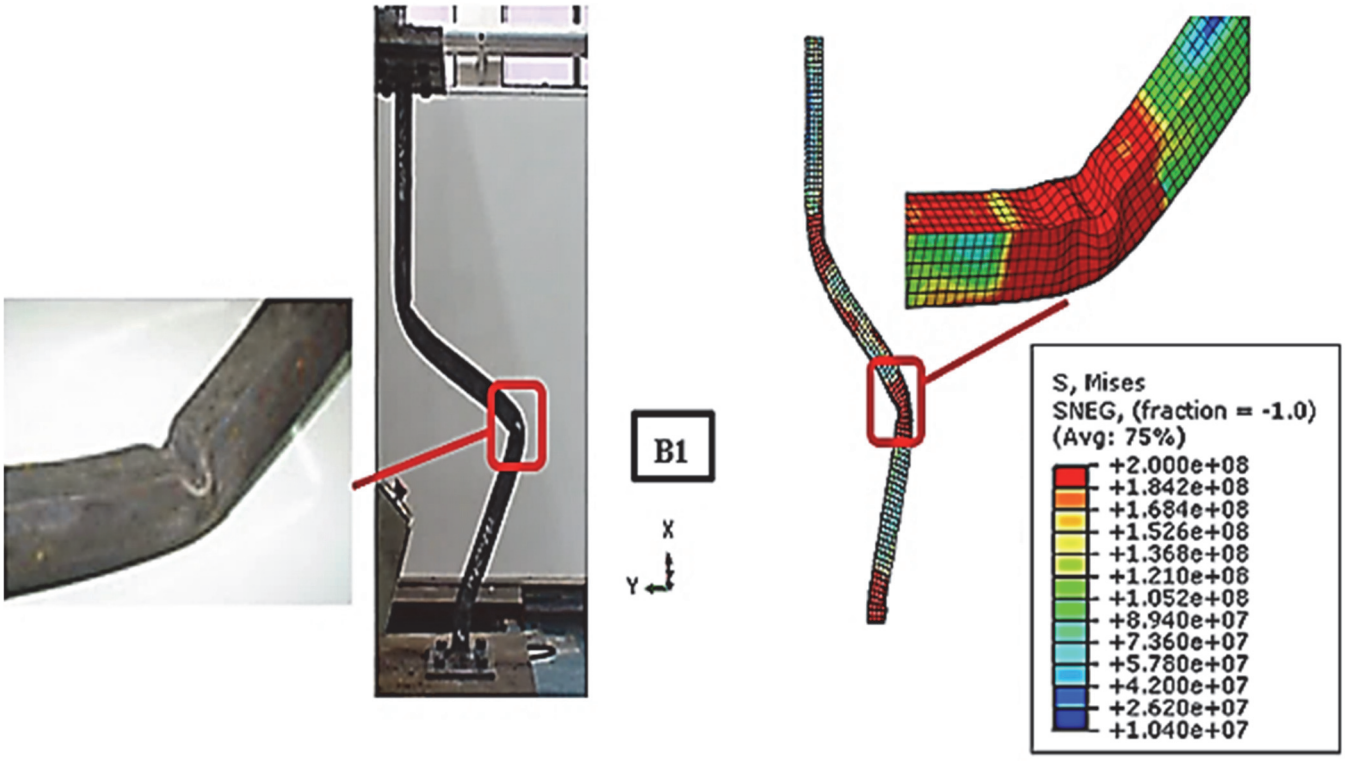

(d)

Figure 6: Comparison of experimental and numerical results showing von Mises stress distributions and failure zones of specimens: a) A1; b) A2; c) A3; d) B1.

CASE STUDY

Using the validated FE model a parametric study is conducted on full scale square and circular hollow section steel column of L = 4000 mm length and t= 2 mm wall thickness of varying section width C (diameter for circular shape) , Curve angle θ , Radius of Curvature R, and the End Parts Offset D as shown in Fig.7 and Fig. 3 . In order to identify key design parameters affecting the load capacity of double curvature hollow structural columns. Since no design code explicitly specifies the optimal section dimensions for the present case, the chosen geometrical details of all tested specimens and steel properties are provided in Tab. 3. Following the methodology proposed in the previous study by A. Khalkhali et al. [17] , The effect of each parameter is assessed through a controlled parametric approach, where only one parameter is altered at a time, keeping the rest unchanged.

The analysis of the results will focus on the ultimate load capacity, the load–displacement behavior along the vertical axis, and the observed failure mechanisms in different positions along the column as pointed in Fig.8, so the next section presents a comparative analysis based on reference specimens outlined in Tab. 3. For the square hollow section, the specimen labeled 'S1-C1-D1-R1' represents a column with a cross-sectional width of 300 mm, an end-part offset of 1000 mm, a curvature radius of 900 mm, and a bending angle of 20°. In contrast, the baseline for the circular hollow section-denoted 'CR1-C1-D1-R1' features a diameter of 509 mm, while maintaining identical values for the offset distance, curvature radius, and curvature angle.

RESULTS AND DISCUSSION

Influence of curvature angle

To investigate the influence of the curvature angle on the structural performance of the hollow steel columns, a range of angles specifically :20°, 25°, 30°, and 35° was selected for the analysis. These values were chosen to cover a representative spectrum of possible curvatures encountered in practice. The numerical results corresponding to

these variations, highlighting their effect are shown in Fig. 9a for the square hollow section and in Fig.9b for the circular hollow section.

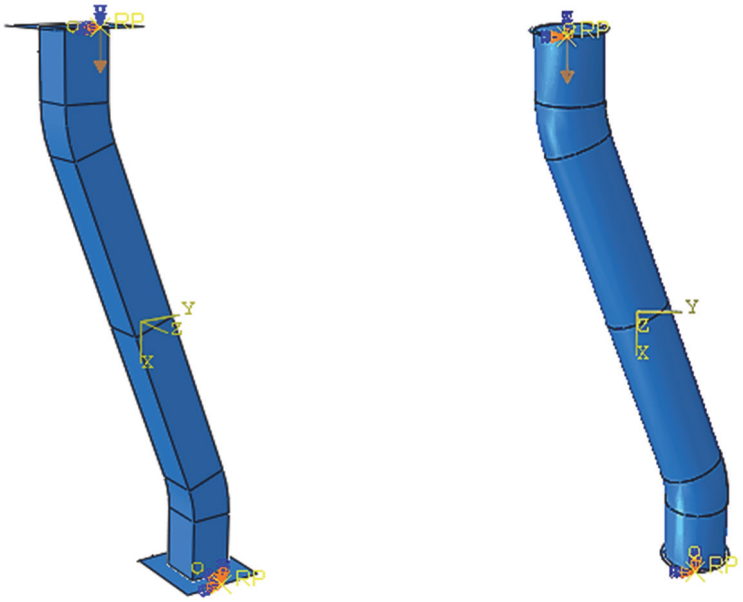

Figure 7: Tested specimens' simulation.

Specimen	L (mm)	T (mm)	C (mm)	D (mm)	R (mm)	Θ (deg)	Fy (MPa)	E (GPa)
S1-C1-D1-R1	4000	2	300	1000	900	20	400	210
S2-C2-D1-R1	4000	2	350	1000	900	20	400	210
S3-C3-D1-R1	4000	2	400	1000	900	20	400	210
S4-C4-D1-R1	4000	2	250	1000	900	20	400	210
S5-C1-D1-R1	4000	2	300	1000	900	25	400	210
S6-C1-D1-R1	4000	2	300	1000	900	30	400	210
S7-C1-D1-R1	4000	2	300	1000	900	35	400	210
S8-C1-D2-R1	4000	2	300	800	900	20	400	210
S9-C1-D3-R1	4000	2	300	600	900	20	400	210
S10-C1-D4-R1	4000	2	300	400	900	20	400	210
S11-C1-D1-R2	4000	2	300	1000	1100	20	400	210
S12-C1-D1-R3	4000	2	300	1000	700	20	400	210
S13-C1-D1-R4	4000	2	300	1000	500	20	400	210
CR1-C1-D1-R1	4000	2	509	1000	900	20	400	210
CR2-C2-D1-R1	4000	2	445	1000	900	20	400	210
CR3-C3-D1-R1	4000	2	381	1000	900	20	400	210
CR4-C4-D1-R1	4000	2	318	1000	900	20	400	210
CR5-C1-D1-R1	4000	2	509	1000	900	25	400	210
CR6-C1-D1-R1	4000	2	509	1000	900	30	400	210
CR7-C1-D1-R1	4000	2	509	1000	900	35	400	210
CR8-C1-D2-R1	4000	2	509	800	900	20	400	210
CR9-C1-D1-R1	4000	2	509	600	900	20	400	210
CR10-C1-D1-R1	4000	2	509	400	900	20	400	210
CR11-C1-D1-R1	4000	2	509	1000	1100	20	400	210
CR12-C1-D1-R1	4000	2	509	1000	700	20	400	210
CR13-C1-D1-R1	4000	2	509	1000	500	20	400	210

Table 3: Geometric details of tested specimens as defined in Fig. 3.

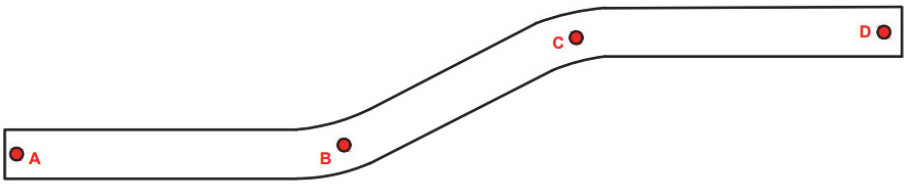

Figure 8: Schematic layout of deformed regions.

A progressive reduction in the maximum load capacity was observed as the curvature angle increased, for both square and circular hollow sections. Specifically, for the square-section specimens labeled 'S5-C1-D1-R1', 'S6-C1-D1-R1', and 'S7-C1-D1-R1', the maximum load dropped by approximately 20.64%, 34.77%, and 41.66%, respectively. When compared to the reference case 'S1-C1-D1-R1' A similar trend was noted for the circular-section 'CR5-C1-D1-R1', 'CR6-C1-D1-R1', and 'CR7-C1-D1-R1', which exhibited reductions of 31.91%, 44.73%, and 58.66%, respectively in comparison with specimens 'CR1-C1-D1-R1'.These results clearly demonstrate that increasing the curvature angle significantly compromises the load-bearing capacity of both section types. These confirm the previous obtained results in the experimental test conducted by A. Khalkhali and al. [17].With respect to the load–displacement response, it is evident that the elastic stiffness was significantly affected, particularly in the case of circular sections as the curvature angle increased. Notably, the displacement corresponding to the peak load was progressively delayed with each increment in curvature angle for the circular hollow specimens. During the post-peak load phase, it was observed that in square hollow section columns, the load–displacement curves diverged significantly, even with a relatively modest reduction in peak load. In contrast, the curves for circular sections remained closely aligned despite variations in curvature angle.

This behavior suggests that square columns offer greater stiffness and resistance to deformation under axial compression. As illustrated in Fig. 10, plastic hinges were observed at different locations depending on the specimen configuration appearing in distinct regions. For the specimens 'S1-C1-D1-R1' and 'CR1-C1-D1-R1', stress concentration was primarily concentrated in the straight segment at points A and D. The stress concentration was then altered to the points A, B and C for specimen 'S1-C1-D1-R1' and B, C and D for specimen 'CR1-C1-D1-R1' leading to plastic hinge formation and local buckling initiation. In the last loading step it can be seen from Fig.10 that buckling failure mode of specimen 'S1-C1-D1-R1' was in the prismatic segment A-B, this last deformed shape was accompanied by the slight local buckling in the C region in accordance with the failure mode reported by A. Khalkhali et al. [17]. Contrary to 'CR1-C1-D1-R1' the buckling failure mode was in the C-D portion (the base of the column) with the buckling of the curved zone B. This confirm that buckling failure mode was not in three positions as previously seen in the experimental test [17] (two in the curved zones and one in the base). One potential explanation for this difference in failure modes pertains to the abbreviated linear regions A-B and C-D observed in these two specimens. In contrast, for specimens 'S5-C1-D1-R1' and 'CR5-C1-D1-R1', buckling initiation was seen in regions B and C as well as in the straight portion portions A-B and CD respectively. Increasing the compressive load lead to same failure mode of the reference specimens, this can be clearly observed in Fig 10. Although the 25° curvature angle caused a substantial decrease in load-bearing capacity, the resulting failure mechanism was nearly identical to that observed in reference specimens. For the specimens 'S6-C1-D1-R1' and 'CR6-C1-D1-R1', the onset of local buckling was predominantly located within the curved sections. Following load enhancement, local buckling initiated at the third position - specifically in zone A for specimen 'S6-C1-D1-R1' and zone D for 'CR6-C1-D1-R1' - ultimately resulting in a final failure mode distributed across three distinct locations. This behavior closely matches the experimental observations reported by Khalkhali et al. [17]. This confirm that enhancing the angle curve to 30 degrees not only affect the stiffness and the capacity load of the column, the stress concentration was altered to the transition zones between straight and curved tube segments (B and C regions). Local buckling phenomena were also identified at distinct critical locations - specifically at point A in specimen 'S6-C1-D1-R1' and point D in 'CR6-C1-D1-R1'. This spatial variation in third-position buckling manifestations suggests fundamentally different stress redistribution patterns between circular and rectangular cross-sectional geometries under loading conditions. The rectangular section exhibited incomplete stress transfer to the lower regions, resulting in predominant stress concentration near the column's upper portion (points A and B). In contrast, the circular profile demonstrated more effective load redistribution from upper to lower zones (points C and D). This distinct stress distribution behavior accounts for the observed divergence in ultimate load capacity, despite near-identical cross-sectional areas between both geometric configurations. The specimens with a 35° curvature angle namely, 'S7-C1-D1-R1' (square section) and 'CR7-C1-D1-R1' (circular section) both exhibited a distinct tripartite local buckling pattern occurring simultaneously in three critical regions (B, C, and D). Despite their different cross-sectional shapes, both specimens failed in almost identical modes, which strongly suggests that the curvature-induced instability dominated the collapse mechanism, overriding the geometric

distinctions between circular and square profiles. At high curvature angles, the geometric imperfection introduced by double curvature significantly amplifies second-order effects and leads to global instability that manifests uniformly across different cross-sectional shapes. In other words, when the curvature reaches or exceeds 35°, the deformation and stress distribution become increasingly governed by the bending curvature and end eccentricities, rather than by the shape of the cross section itself. This convergence in failure behavior indicates that beyond this curvature threshold, the local geometric features (edges, corners, curvature continuity) no longer play a decisive role in the buckling pattern.

The variation in the number and placement of buckling indicates differences in how internal stresses are distributed depending on the specimen angle curvature, this suggests that angle curvature significantly influences the stress distribution and deformation pattern, curved segments become the critical regions as the curvature angle increases. Decreased curvature angles facilitate effective utilization of the offset distance at column extremities, thereby enhancing structural performance. Specifically, reduced angular deformation enables active participation of end-zone geometry in load-bearing mechanisms and improved stress distribution throughout the member length, which increased composite action between curved and straight segments.

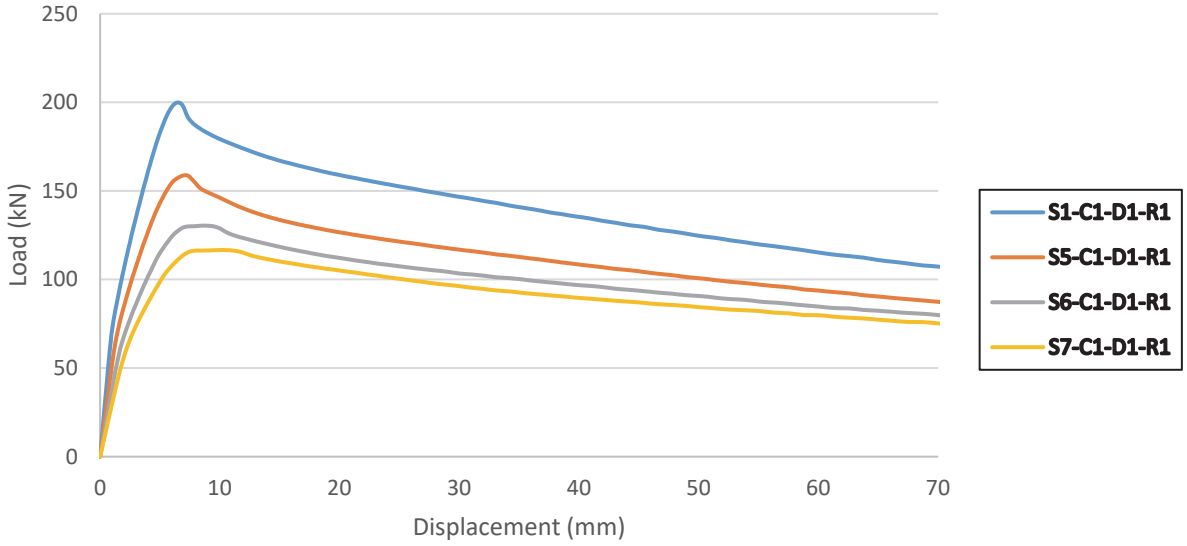

(a)

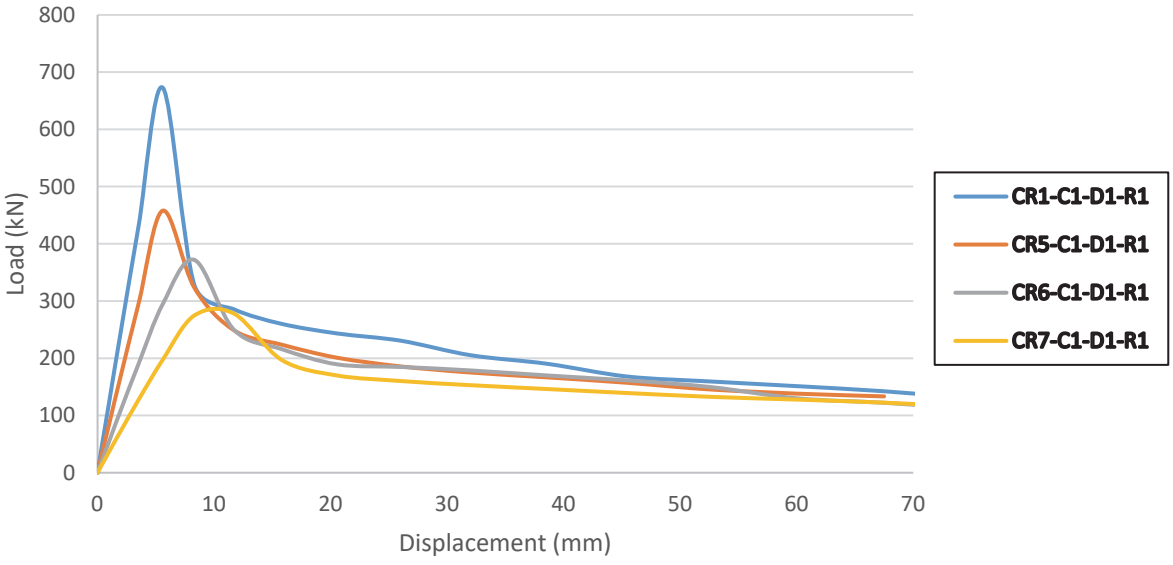

(b)

Figure 9: Load–Deflection Behavior of: (a) Square Sections with different angle curvatures and (b) circular sections with different angle curvatures.

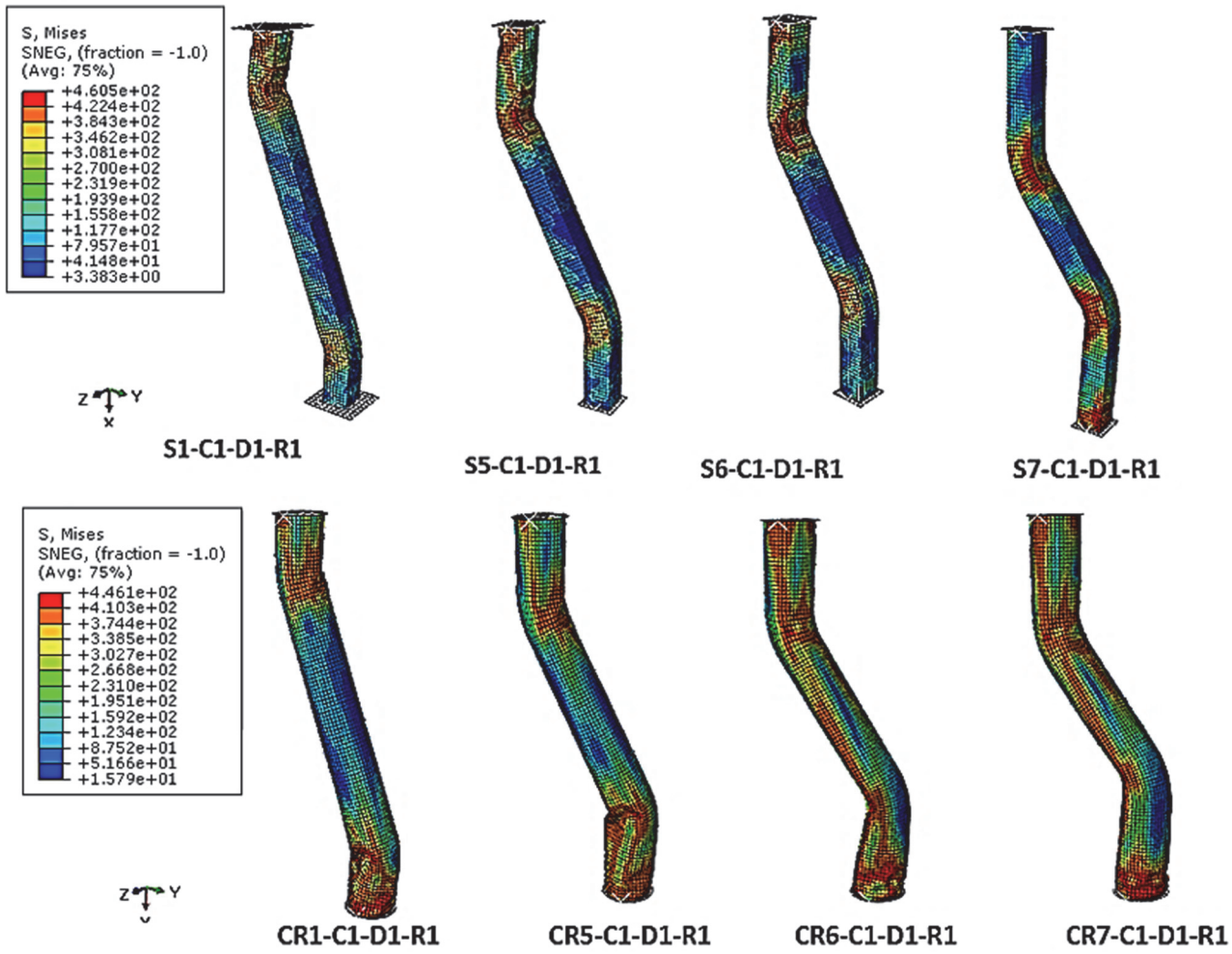

Figure 10: Failure Patterns of tested specimens with different angle curvatures.

Influence of transverse dimensions

In this section, the influence of the cross-sectional width defined as the web width C for square hollow sections and the diameter for circular hollow sections is investigated. For the square configuration, four different widths were examined: 250 mm, 300 mm, 350 mm, and 400 mm. In the case of circular sections, the corresponding diameters considered were 318 mm, 381 mm, 445 mm, and 509 mm. These variations were selected to assess how the increase or decrease in transverse dimensions affects the overall structural behavior and load-carrying capacity under axial compression.

For square hollow section columns, a moderate increase in peak load was recorded approximately 5% for specimen 'S2-C2-D1-R1' and 10% for 'S3-C3-D1-R1'. In contrast, specimen 'S4-C4-D1-R1' showed a slight decrease of about 7.5% compared to the reference configuration. On the other hand, the circular section columns exhibited a clear reduction in maximum load capacity, with decreases of around 11%, 31%, and 71% for specimens 'CR2-C2-D1-R1', 'CR3-C3-D1-R1', and 'CR4-C4-D1-R1', respectively. The obtained results revealed also an interesting divergence in structural performance between geometric profiles, despite that square section columns exhibited only marginal reduction in ultimate load capacity their stiffness characteristics remained essentially unchanged maintaining comparable values to control sample 'S4-C4-D1-R1' across all tested configurations. This preservation of stiffness properties suggests that the square profile's inherent geometric properties provide consistent resistance to deformation regardless of to the additional moments created by loading conditions and geometric form of this type of columns. In contrast, circular section specimens demonstrated markedly different behavior, as evidenced in Figs11 and 12. These members showed progressive stiffness degradation that varied significantly with the diameter of the section. The 'S4-C3-D1-R1' specimen configuration proved to be the least effective in maintaining structural stiffness, suffering the most severe rigidity deterioration under loading conditions. This extreme response likely results from an unfavorable interaction between its specific curvature and diameter-to-thickness ratio creating a suboptimal stress distribution pattern. The observed disparity in stiffness reduction may be attributed to

fundamental differences in moment of inertia characteristics and buckling resistance properties of the studied sections, this was found in previous researches on hollow section columns [22].

Regarding the failure mode of tested columns, from the simulation in the software it was possible to track real-time strain mapping revealed the progressive nature of stress transfer, demonstrating how load paths evolved during deformation. During the initial loading phase, as previously mentioned, distinct stress concentration patterns were observed in specimens 'S1-C1-D1-R1' and 'CR1-C1-D1-R1'. The stress distribution initially localized at terminal points A and D before progressively migrating toward the curved regions B and C. This phenomenon demonstrates the characteristic load-path behavior of curved structural members, where stress transmission follows a sequential pattern from straight segments to curved zones. Similar stress transfer mechanisms were highlighted in the previous investigation [17]. As loading intensified to subsequent stages, a notable third stress concentration developed, returning to the initial points (A and D) in both specimen types indicating the buckling initiation in these regions. After those results demonstrated clear buckling propagation patterns during the plasticization phase for both specimen geometries. In the circular profile 'CR1-C1-D1-R1', a progressive buckling wave developed continuously between points C and D, indicating a stable post-yield collapse mechanism. This propagation behavior suggests complete participation of the entire segment in the failure process through sequential plastic hinge formation. The rectangular specimen 'S1-C1-D1-R1' showed comparable but geometrically influenced behavior, with buckling concentrated along the A-B segment rather than the C-D path observed in the circular section. Both specimens exhibited directional buckling propagation despite their different cross-sectional shapes, confirming that plasticization-phase collapse follows predictable paths once initiated. The circular section's radial symmetry promoted uniform stress redistribution during buckling progression, while the rectangular profile's orthogonal planes created preferential failure directions. Failure patterns across specimens with modified transverse dimensions, demonstrating remarkable similarity to the failure modes observed in previous angle variations of identical specimen configurations. This persistent behavioral correspondence suggests that dimensional alterations within the tested range ('S1-C1-D1-R1','CR1-C1-D1-R1') exerted negligible influence on the fundamental failure mechanism as shown in Fig.13, despite that it was more significant in load carrying capacities. Regarding specimens 'S2-C1-D1-R1' and 'CR2-C1-D1-R1' revealed consistent failure patterns characterized by localized buckling in specific segments. For the rectangular profile 'S2-C1-D1-R1', buckling deformation consistently initiated and propagated within segment AB, while the circular counterpart 'CR2-C1-D1-R1' exhibited similar behavior concentrated in segment CD. Notably, both configurations demonstrated complete absence of buckling phenomena in the third curved regions, providing compelling evidence for the efficacy of the implemented transverse section. Specimen 'S3-C1-D1-R1', which exhibited the highest ultimate load capacity among all tested configurations, ultimately failed through buckling of the straight segment CD, see Fig.13. This failure pattern provides critical insights into the mechanical behavior of geometrically enhanced square sections. The observed collapse mechanism indicates that increasing the transverse dimensions of the square cross-section fundamentally altered the column's stress distribution characteristics. Specifically, the dimensional modifications appear to have shifted the primary stress concentration zone toward the lower region of the column and created conditions favorable for buckling initiation in the bottom segment. This behavioral pattern strongly suggests that the enhanced cross-section provided sufficient flexural stiffness to effectively transfer applied loads from the top to the base of the member. The capacity to maintain stress redistribution throughout the column height until ultimate failure confirms the improved load transfer efficiency achieved through transverse dimension augmentation. Furthermore, the localization of buckling in segment CD, rather than in other regions, demonstrates that the section modifications successfully controlled the failure location while simultaneously increasing overall load-bearing capacity. The investigation revealed also consistent failure mechanisms in specimens 'CR3-C3-D1-R1' and 'S4-C4-D1-R1', maintaining identical collapse patterns despite modifications to their transverse section dimensions. This behavioral consistency suggests that while dimensional alterations significantly influenced load-bearing capacity, particularly in the circular profile which demonstrated variation in ultimate load, they did not fundamentally alter the underlying failure mode. Significant stress distribution pattern for specimen 'CR4-C4-D1-R1', characterized by pronounced stress concentrations extending along the entire member length. This uniform stress intensification ultimately precipitated buckling failure localized at the column base. These results highlight the behavior of double curved structural columns under compressive loading. A partial decoupling between load-bearing capacity and failure mechanisms, where geometric modifications significantly influence ultimate strength while maintaining consistent collapse patterns across specimen variations. This phenomenon suggests that while cross-sectional parameters primarily govern load capacity through their effect on stress distribution and moment resistance as reported by Hilo et al. [4], the failure modes remain predominantly determined by global structural characteristics such as overall curvature and boundary conditions. An optimal design of curved structural elements requires balanced consideration of both cross-sectional strength properties and system-level stability behavior, with particular attention to regions prone to secondary moment accumulation. Subsequent investigations should consequently explore the interdependent effects of curvature radius and end-offset dimensions.

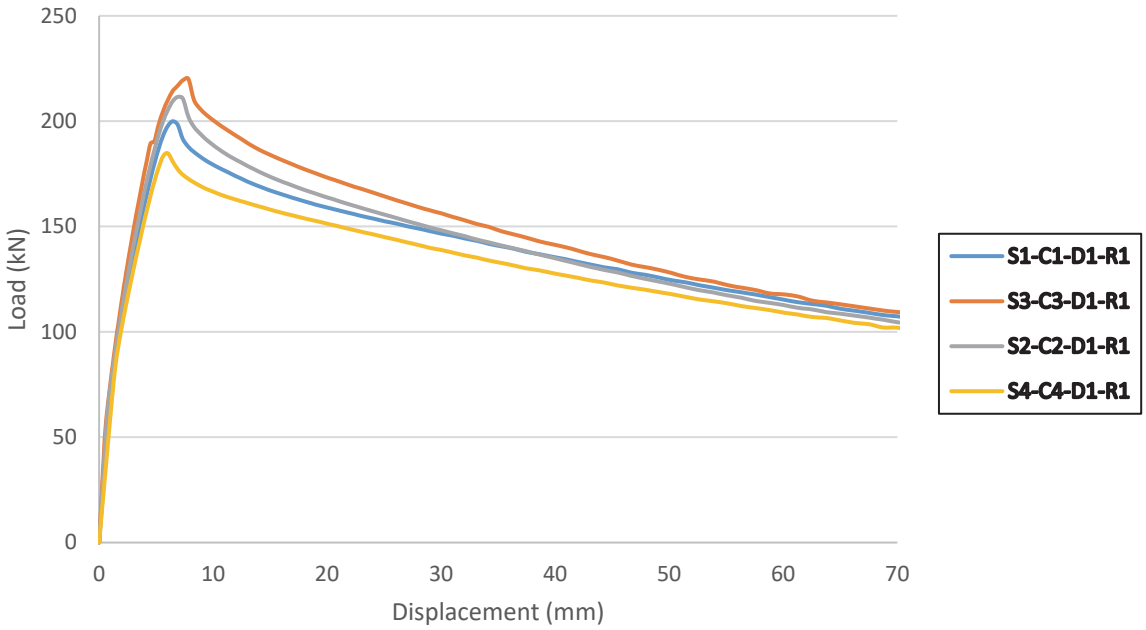

Figure 11: Load–Deflection Behavior of Square Sections with different web width.

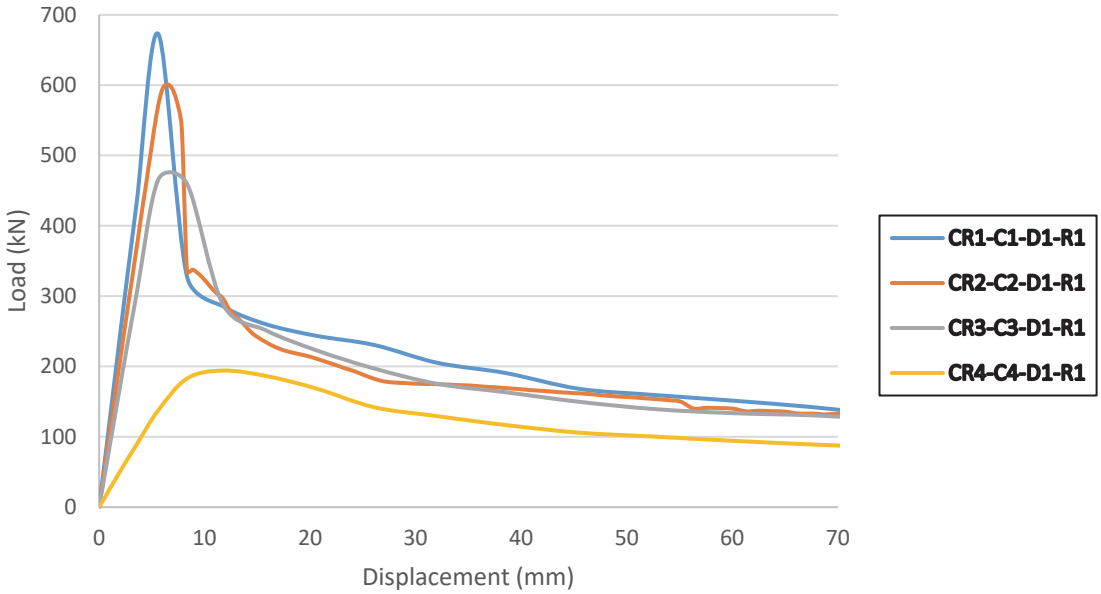

Figure 12: Load–deflection behavior of circular sections with different diameter width.

Influence of the radius of curvature

The numerical investigation systematically evaluated curvature radius effects on double curved steel columns performance through a carefully designed parametric study encompassing four geometrically distinct configurations: 500 mm, 700 mm, 900 mm, and 1100 mm. Results demonstrated remarkable consistency in structural response across the entire curvature spectrum, with peak load variations remaining below 2.5% between extreme cases, as quantitatively evidenced in Figs. 13 and 14. This radius-independent behavior manifested through three key observations: first, nearly identical elastic stiffness values; second, consistent nonlinear deformation patterns during plastic hinge formation; and third, uniform stress redistribution mechanisms regardless of curvature severity. The load-displacement curves exhibited parallel post-yield trajectories with less than 3% divergence, confirming that curvature radius becomes a secondary design parameter within

the investigated range. These findings corroborate and technically extend Khalkhali et al. [17] fundamental work by providing quantitative validation of curvature insensitivity through advanced strain mapping techniques.

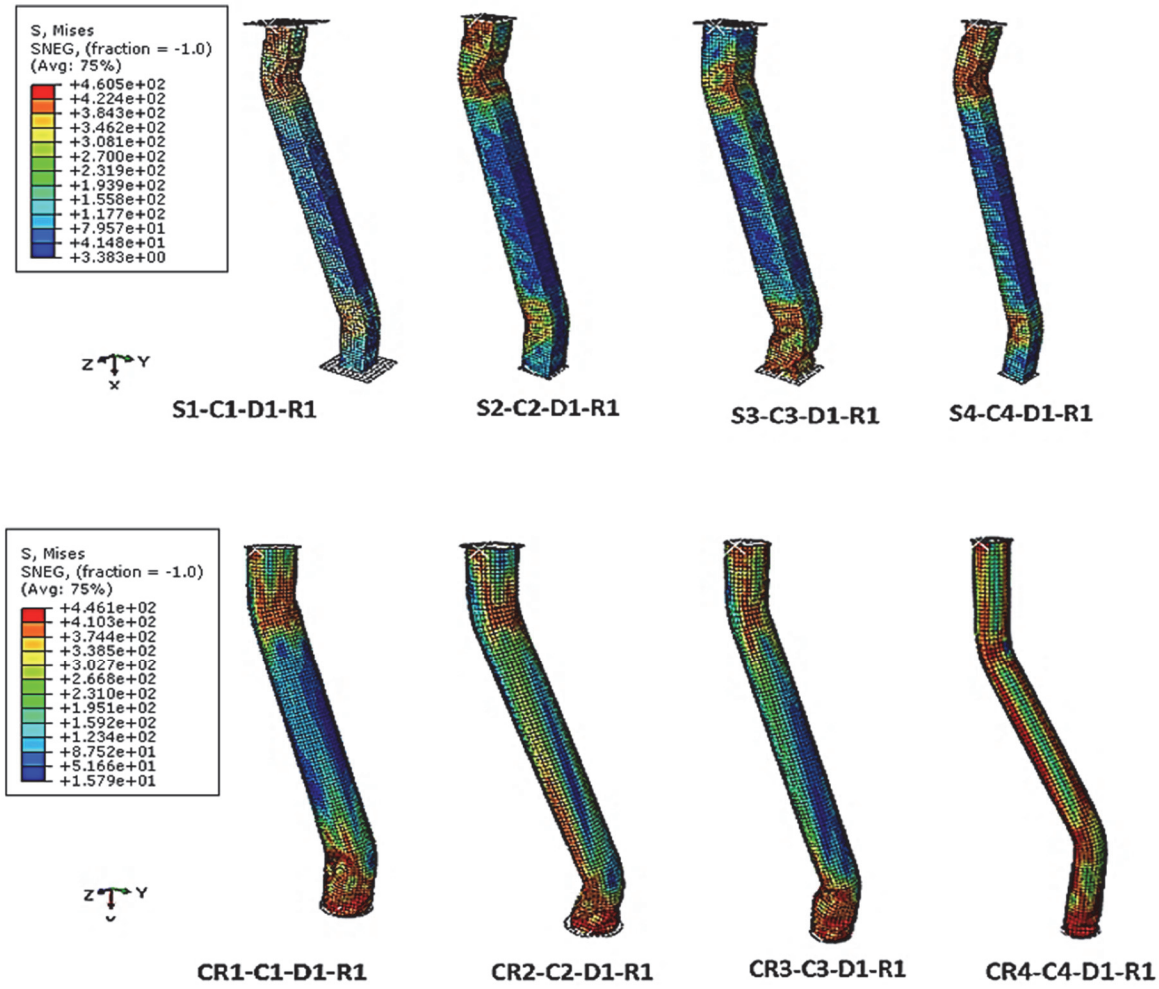

Figure 13: Failure Patterns of tested specimens with different sections.

Failure modes in square hollow section columns reveal a complex interplay between geometric parameters and structural behavior, as evidenced by the detailed analysis of Fig. 16. While the global collapse mechanism maintained fundamental similarities with reference specimens, sophisticated digital image correlation techniques uncovered significant variations in stress distribution patterns that fundamentally alter our understanding of curved member performance. The specimen S12-C1-D1-R4 exhibited a remarkable phenomenon of stress migration, where the primary concentration zone progressively shifted from the conventional upper segment AB to the lower region CD during the loading sequence. This transition, which initiated at approximately 72% of the ultimate load capacity, suggests a fundamental change in load path mechanics that challenges conventional column design assumptions. Advanced strain mapping demonstrates that this stress redistribution occurred through three distinct phases: initial elastic stress concentration in segment AB followed by progressive transfer of compressive stresses to segment CD, and final localization of plastic strains in the lower region leading to collapse. In contrast, specimen CR11-C1-D1-R1 displayed a more complex failure sequence characterized by simultaneous plastic hinge formation in both the upper curved segment and adjacent straight portion. This dual-hinge mechanism created a unique collapse scenario where initial yielding developed in the curved region at 65% of peak load, followed by secondary plastic hinge formation in the straight segment at 82% load capacity. The final failure mode involved localized buckling at top and bottom curvature segment (AB and CD. This failure patterns result from complex interactions between geometric discontinuities and material plasticity.

The interaction between these failure mechanisms suggests that curved members develop a distributed plasticity pattern that differs fundamentally from straight column behavior. These observations align with those reported by Mohammed et al. [16]. It should be noted that these results demonstrate an important dichotomy in structural behavior: while variations in

curvature radius produced statistically insignificant changes in compressive load capacity, they significantly modified failure mechanisms through systematic redistribution of stress concentrations. Comparative analysis revealed consistent migration of critical stresses from segment AB to CD in modified specimens, with some configurations developing balanced stress distribution across both segments in contrast to reference specimens. This provides empirical validation for incorporating end-offset segments in design to participate to the column resistance, as they enhance structural efficiency through active participation in load transfer mechanisms. Promote favorable stress redistribution away from critical curvature transition points (B and C). Since all tested specimens in this study that failed by the plasticization of the curved regions demonstrated a dramatic decrease in stiffness and load carrying capacities.

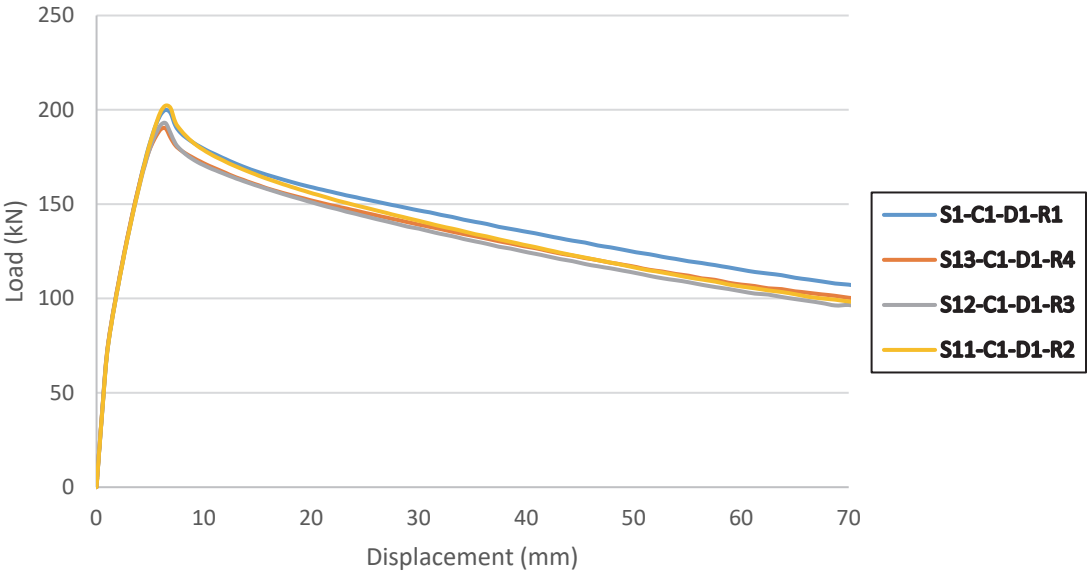

Figure 14: Load–Deflection behavior of square sections with different values of radius curvature.

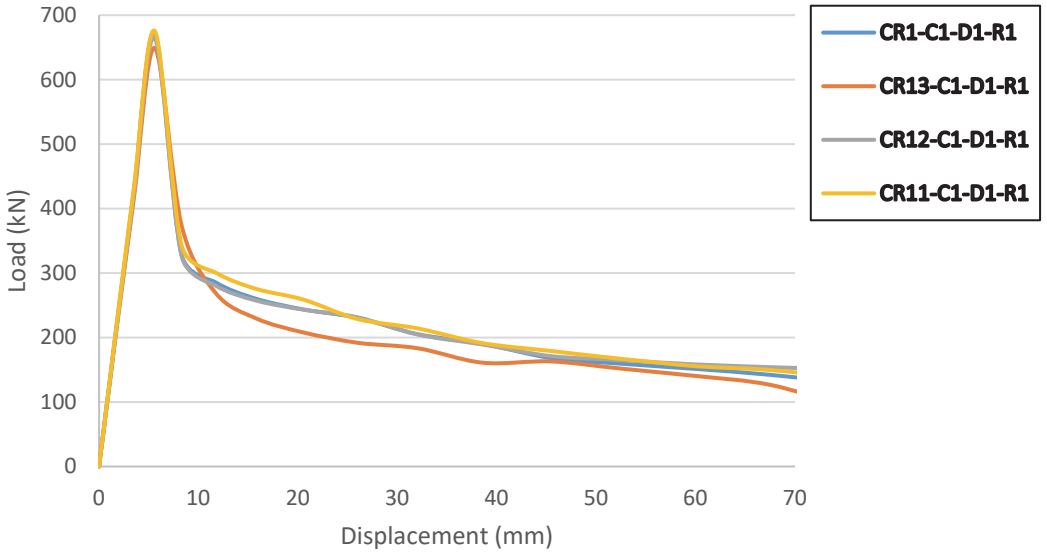

Figure 15: Load -Deflection behavior of circular sections with different values of radius curvature.

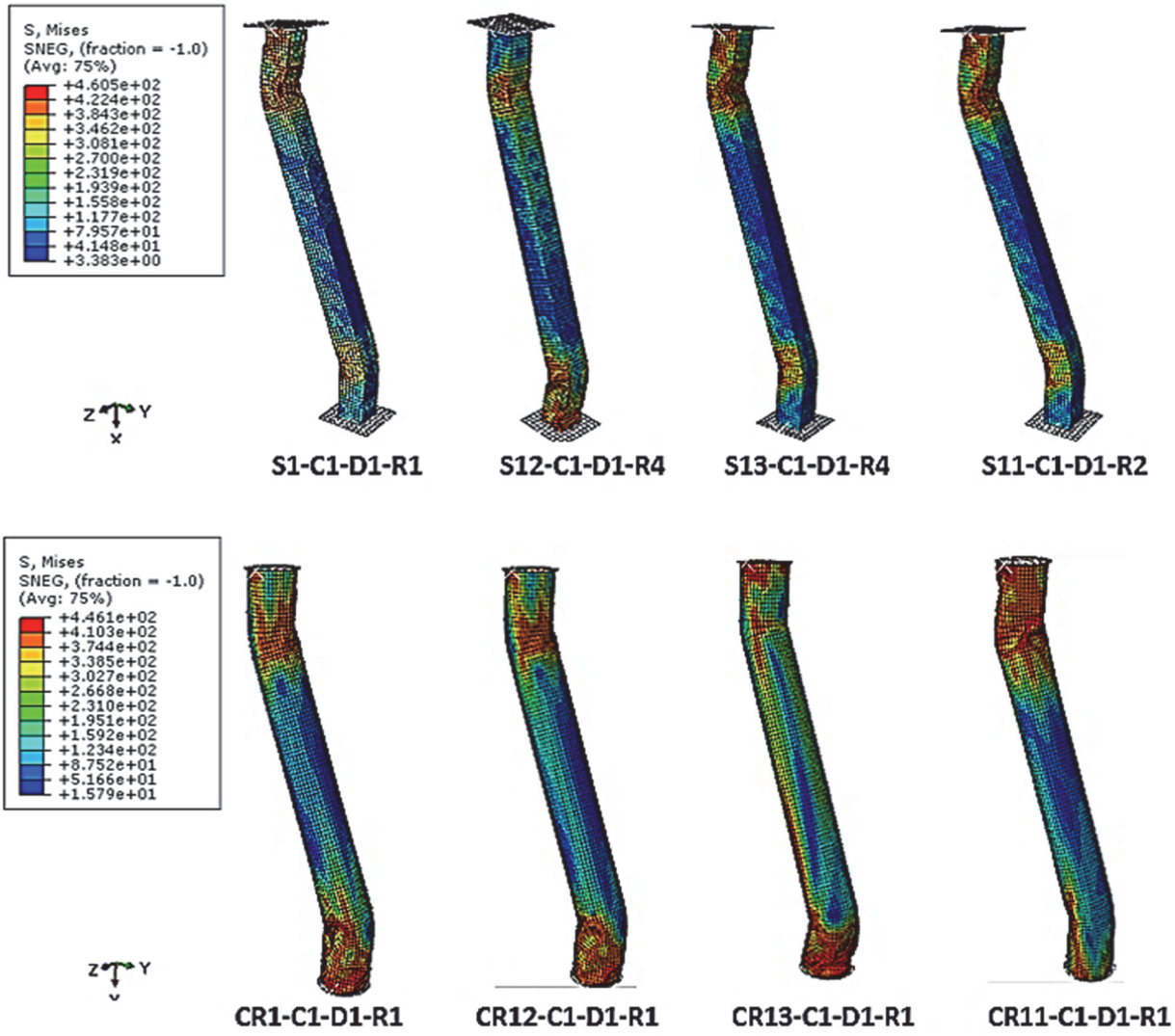

Figure 16: Failure patterns of tested specimens with different radius of curvature.

Influence of offset distance at column ends

By systematically varying the offset distance D of the end parts to values of 1000 mm, 800 mm, 600 mm, and 400 mm, significant and distinct behavioral variations were observed between square and circular hollow section columns. Compared to the reference specimens, the peak load experienced a reduction ranging from 13% to 21% for the square sections, and from 15% to 37% for the circular ones (Figs 17 and 18). It can also be seen that an examination of the data reveals that specimens 'S8-C1-D2-R1', 'S9-C1-D3-R1', and 'S10-C1-D4-R1' demonstrated a decline in peak load, adhering to a linear pattern comparable to that observed in specimens 'CR8-C1-D2-R1', 'CR9-C1-D2-R1', and 'CR10-C1-D2-R1', albeit with a more pronounced reduction in load-bearing capacity. To optimize the design of double-curved steel hollow columns, the offset distance at the column ends should not exceed a certain threshold decrease, as it directly influences the load-bearing capacity particularly in circular cross-sections. An analysis of the initial stiffness characteristics revealed that specimens 'S8-C1-D2-R1', 'S9-C1-D3-R1', and 'S10-C1-D4-R1' demonstrated close alignment with the reference specimen, indicating consistent structural behavior under comparable loading conditions. However, a progressive reduction in the offset distance (D) to 800 mm and 600 mm was found to significantly influence structural performance, manifesting as a marked decline in stiffness for modified specimens 'CR9-C1-D2-R1' and 'CR10-C1-D2-R1', respectively. This observed trend suggests an inverse relationship between offset distance and stiffness retention, where diminished cross-sectional spacing directly contributes to reduced load redistribution efficiency. The pronounced stiffness degradation in specimens with reduced offset distances underscores the importance of maintaining optimal geometric parameters in the design of hollow steel columns to preserve structural integrity under service loads.

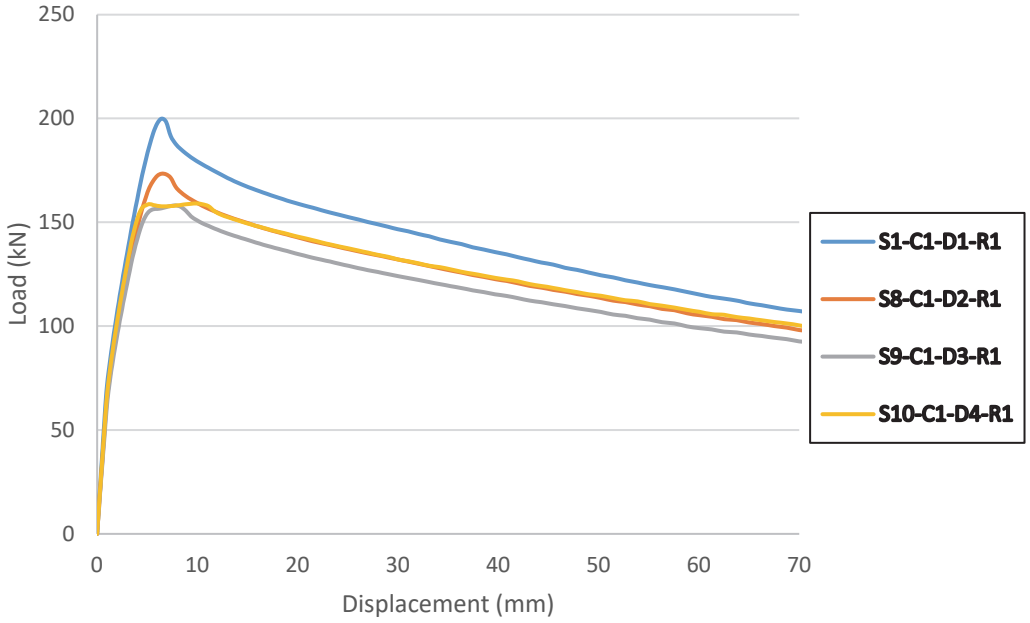

Figure 17: Load–Deflection Behavior of square sections with different values of end Parts offset.

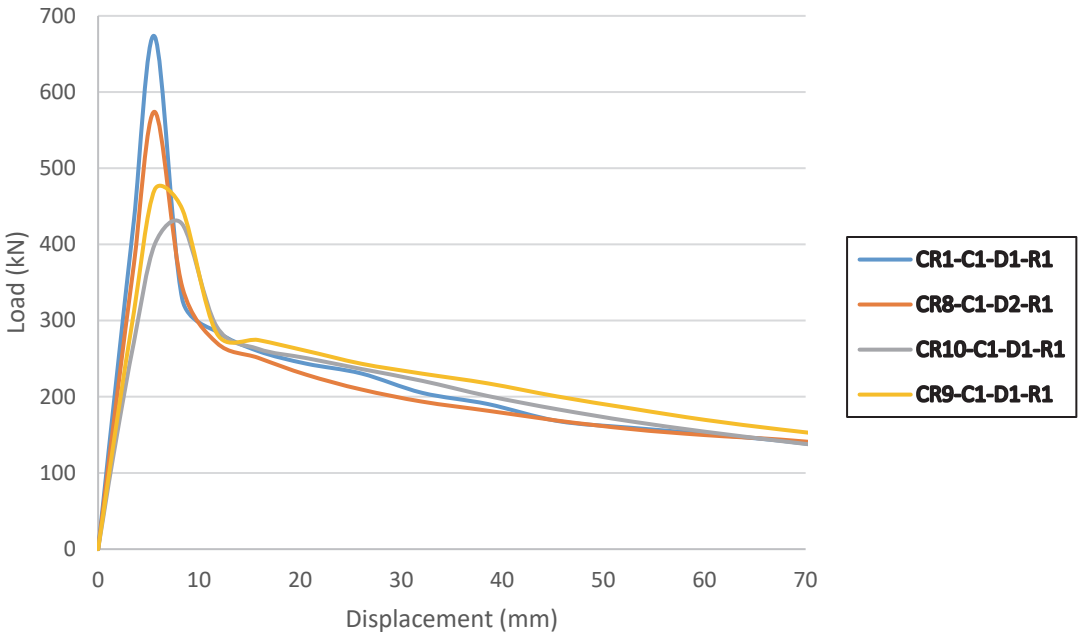

Figure 18: Load–Deflection Behavior of circular sections with different values of end Parts offset.

The failure mechanisms of double-curved hollow steel columns revealed critical behavioral patterns associated with varying offset distances. Specimens configured with end part offsets of 600 mm and 400 mm consistently demonstrated the development of plastic hinges at both curved regions (B and C) during loading, this can clearly be seen in Fig.19. This phenomenon was systematically observed in both square hollow section and circular hollow section column configurations, indicating a fundamental structural response tied to reduced offset dimensions rather than being section-dependent. The formation of plastic hinges at these reduced offset distances suggests a significant alteration in the moment distribution along the column length. As the offset distance decreases, the curvature intensity in the bent regions increases substantially. This heightened curvature induces greater strain localization, which in turn accelerates the onset of yielding and subsequent

plastic hinge formation. The correlation between offset reduction and enhanced plastic deformation was further evidenced by the measured collapse angles, which exhibited a marked increase in specimens with shorter offsets. This observation implies that the deformation capacity becomes more concentrated in the curved zones as the offset diminishes. From a mechanistic perspective, the pronounced inelastic behavior observed in specimens with shorter offsets can be attributed to several interrelated factors. First, the reduced offset length creates a more abrupt change in stiffness at the curved sections, leading to stress concentration effects. Second, the decreased moment arm between curved segments alters the load path, resulting in higher bending moments being transferred to these critical regions. Third, the geometric constraints imposed by smaller offsets limit the column's ability to redistribute stresses, thereby localizing deformation. It should be noted also that specimens 'CR9-C1-D2-R1' and 'CR10-C1-D2-R1' demonstrate a more ductile failure mode characterized by extensive plastic deformation in the curved zones (B and C). This behavior contrasts with specimens having larger offsets, where failure typically occurs through a combination of local buckling and yielding distributed more evenly along segment AB or CD. This indicates that while reduced offsets may enhance energy dissipation capacity through plastic deformation, they simultaneously reduce the column's overall stability by concentrating damage in curved regions [17]. The current parameter under investigation aligns with previously studied variables through its consistent influence on load distribution mechanisms. The reduction of this particular parameter induces two consequential effects that fundamentally alter structural performance: elongation of straight segments (AB, CD) and intensified stress concentration within curved transition zones. These geometric modifications create a detrimental mechanical scenario where the extended linear segments become progressively less effective in load resistance, effectively functioning as non-participatory parts within the overall structural system. The observed phenomenon manifests through distinct behavioral patterns in test specimens 'CR9-C1-D2-R1', 'CR10-C1-D2-R1', 'S9-C1-D3-R1', and 'S10-C1-D4-R1', all of which exhibited suboptimal performance characteristics.

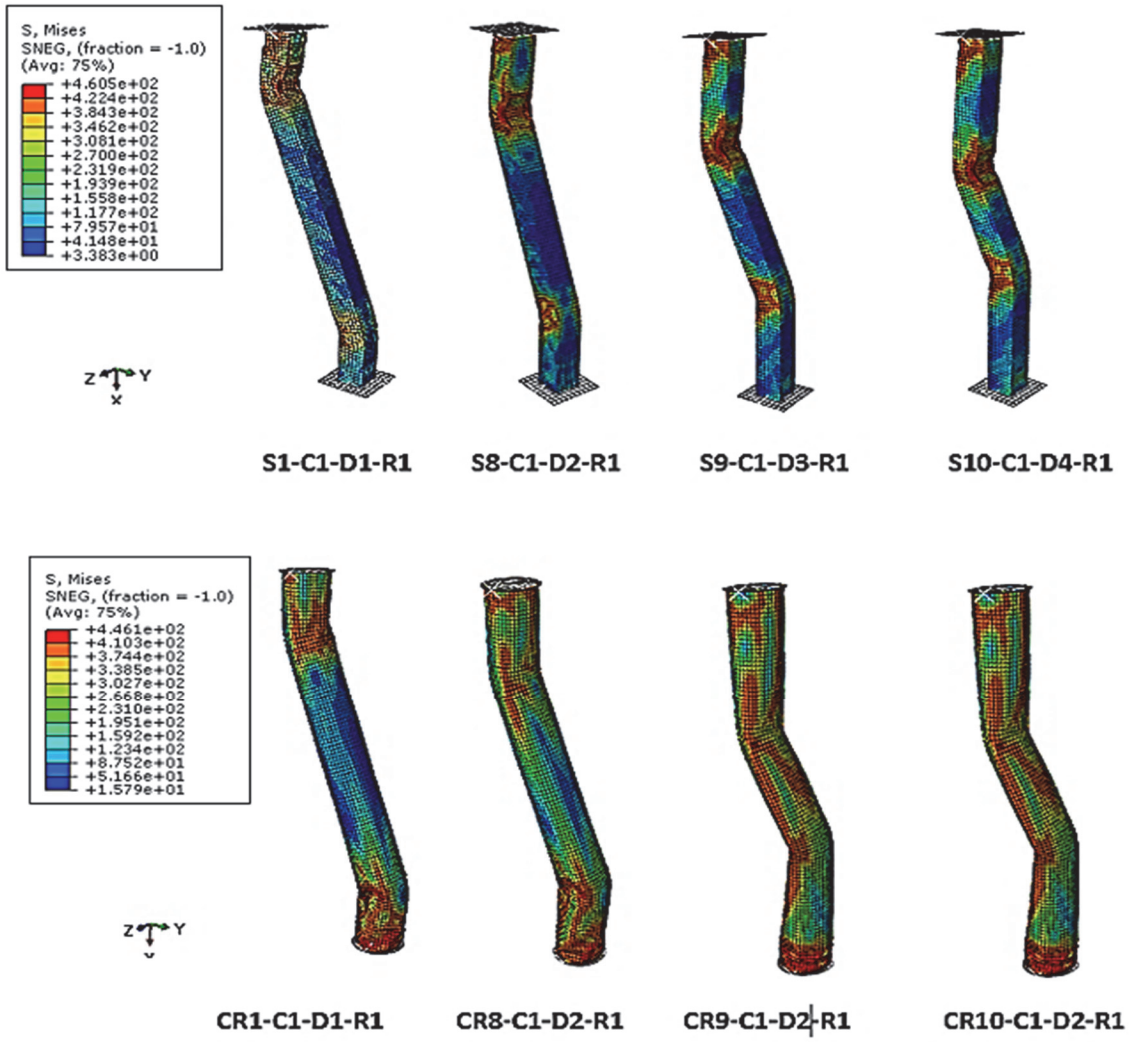

Figure 19: Failure patterns of tested specimens with different values of end parts offset.

Numerous previous studies [23–25] have conclusively demonstrated that enhanced wall thickness significantly improves compressive resistance by delaying the onset of local buckling phenomena a finding that has been widely incorporated into modern design codes. This thickness-dependent behavior primarily stems from increased sectional stiffness, which effectively redistributes stress concentrations and postpones the formation of characteristic buckling modes. However, while these wall thickness considerations remain fundamental to column design, the current investigation deliberately shifts focus toward the less explored domain of geometric curvature effects, thereby addressing a notable gap in existing structural engineering knowledge.

CONCLUSION

Despite the increasing architectural use of double-curvature steel columns, their structural behavior remains largely underexplored in the current literature. This study presents a pioneering numerical investigation aimed at understanding the load-bearing capacity and failure mechanisms of double-curved hollow steel sections under axial compression. The models were developed using ABAQUS finite element software, and the analysis encompassed a wide range of geometric parameters including cross-sectional shape, curvature angle, curvature radius, web width (or diameter), and end offset.

The main conclusions of this study can be summarized as follows:

- Validation of the numerical model: The finite element simulations showed strong correlation with reference experimental results in terms of global load–displacement response and failure modes, thereby confirming the reliability and accuracy of the adopted numerical approach.
- Influence of section shape: Square cross-sections provided higher axial strength compared to circular ones. This was attributed to their greater directional stiffness and reduced susceptibility to local buckling under compressive loads.
- Critical role of geometry: Among all parameters, web width and curvature angle had the most significant influence on failure behavior, particularly for circular profiles. Their impact is directly linked to the way stress concentrations develop and propagate along the curved segments.
- Dominance of end offset: The distance between the column ends and the inflection point of curvature was identified as the most sensitive parameter. A reduction in this offset resulted in substantial performance degradation and earlier onset of instability.
- Influence of curvature radius: The curvature radius, surprisingly, had a minor effect on axial capacity. This finding suggests that, within a reasonable range, the column maintains stiffness and distributes stresses smoothly regardless of the extent of the curvature.
- Failure mechanism characterization: All specimens exhibited a combination of local buckling and plastic hinge formation. However, the location and severity of these phenomena varied depending on the geometric configuration, offering a new classification framework for failure in curved columns.
- Design implications: Optimal performance was obtained for columns combining small curvature angles, larger transverse dimensions, and sufficiently large end offsets. Avoiding failure initiation in the curved zones and confining buckling to straight terminal segments was key to improving structural response.

This work lays a solid foundation for future experimental and numerical studies on architecturally complex steel elements. It also delivers practical guidance for engineers seeking to integrate curved steel members into load-bearing systems while balancing form and function. Further investigations should explore a broader spectrum of materials, cross-sectional shapes (e.g., elliptical, polygonal), connection conditions, and reinforcement strategies to fully unlock the structural potential of double-curved columns.

REFERENCE

[1] Hengsheng, L. (2023). The application and value of curved roof in modern architecture, Appl. Comput. Eng., 12(1), pp. 170–176, DOI: https://doi.org/10.54254/2755-2721/12/20230332.

[2] Made-in-China, "Prefab steel building JTS-002." [Online]. Available: https://id.made-in-china.com/co_zerchen/product_Prefab-Steel-Building-JTS-002-_heueyhuiu.html

[3] Sediek, O.A., Wu, T.-Y., McCormick, J., El-Tawil, S. (2020). Collapse Behavior of Hollow Structural Section Columns under Combined Axial and Lateral Loading, J. Struct. Eng., 146(6),

DOI: https://doi.org/10.1061/(ASCE)ST.1943-541X.0002637.
[4] Hilo, S.J., Sabih, S.M., Faris, M.M., Al-Zand, A.W. (2022). Numerical Investigation on the Axial Load Behaviour of Polygonal Steel Tube Columns, Int. Rev. Civ. Eng., 13(5), pp. 397, DOI: https://doi.org/10.15866/irece.v13i5.20548.
[5] Han, L.-H., Zheng, L.-Q., He, S.-H., Tao, Z. (2011). Tests on curved concrete filled steel tubular members subjected to axial compression, J. Constr. Steel Res., 67(6), pp. 965–976, DOI: https://doi.org/10.1016/j.jcsr.2011.01.012.
[6] Han, L.-H., He, S.-H., Zheng, L.-Q., Tao, Z. (2012). Curved concrete filled steel tubular (CCFST) built-up members under axial compression: Experiments, J. Constr. Steel Res., 74, pp. 63–75, DOI: https://doi.org/10.1016/j.jcsr.2012.02.008.
[7] Zheng, L., Wei, C., Chen, M., Zheng, Y. (2018). Behaviour of circular curved concrete filled stainless steel tubular struts under compression, Xi'an Jianzhu Keji Daxue Xuebao/Journal Xi'an Univ. Archit. Technol., 50, pp. 491–499 and 519, DOI: https://doi.org/10.15986/j.1006-7930.2018.04.005.
[8] Erkoç, Y., Torunbalci, N. (2023). Effect of Architectural Design in Twisted-Form Buildings to Structural System Design, 2, Journal of Science., GU J Sci, Part B, 11(2), pp. 269-282.
[9] Lin, K., Kurata, M., Kawasaki, Y., Kitatani, Y. (2024). Investigation of low-disturbance seismic retrofit method for steel column bases using curved members, JAPAN Archit. Rev., 7(1), DOI: https://doi.org/10.1002/2475-8876.12429.
[10] Pi, Y.-L., Bradford, M.A. (2004). Effects of prebuckling deformations on the elastic flexural-torsional buckling of laterally fixed arches, Int. J. Mech. Sci., 46(2), pp. 321–342, DOI: https://doi.org/10.1016/j.ijmecsci.2004.02.012.
[11] Pi, Y.-L., Trahair, N.S. (1999). In-Plane Buckling and Design of Steel Arches, J. Struct. Eng., 125(11), pp. 1291–1298, DOI: https://doi.org/10.1061/(ASCE)0733-9445(1999)125:11(1291).
[12] AISC, D.G. 33. (2018). Curved Member Design, Bo Dowswell, PE, PhD.
[13] Jolly Monge, D. (2017). New columns for architecture in reinforced concrete, Rev. La Construcción, 16(3), pp. 489–497, DOI: https://doi.org/10.7764/RDLC.16.3.489.
[14] Pi, Y.L., Bradford, M.A. (2003). Inelastic buckling and strengths of steel I-section arches with central torsional restraints, Thin-Walled Struct., 41(7), pp. 663–689, DOI: https://doi.org/10.1016/S0263-8231(02)00094-0.
[15] Wei, J., Wu, Q., Chen, B., Wang, T.-L. (2009). Equivalent Beam-Column Method to Estimate In-Plane Critical Loads of Parabolic Fixed Steel Arches, J. Bridg. Eng., 14(5), pp. 346–354, DOI: https://doi.org/10.1061/(ASCE)1084-0702(2009)14:5(346).
[16] Mohammed, H. (2021). Behaviour of Geometrically Nonlinear Columns: Towards an Accurate Structural Design of Columns Made Using Hot Rolled-Open Steel Section, Acad. J. Eng. Stud., 2(1), pp. 1–9, DOI: https://doi.org/10.31031/aes.2021.02.000529.
[17] Khalkhali, A., Masoumi, A., Darvizeh, A., Jafari, M., Shiri, A. (2011). Experimental and Numerical Investigation into the Quasi-Static Crushing Behaviour of the S-Shape Square Tubes, J. Mech., 27(4), pp. 585–596, DOI: https://doi.org/10.1017/jmech.2011.61.
[18] Dassault Systèmes. (2016). Abaqus 2016, Abaqus/Cae User'S Guide, , pp. 1144.
[19] Kouider, N., Hadidane, Y., Benzerara, M. (2021). Numerical investigation of the cold-formed I-beams bending strength with different web shapes, Frat. Ed Integrità Strutt., 16(59), pp. 153–171, DOI: https://doi.org/10.3221/IGF-ESIS.59.12.
[20] Guedaoura, H., Hadidane, Y. (2022). Web post-buckling strength of thin-webbed cellular beams using carbon PFRP profiles, Frat. Ed Integrità Strutt., 16(60), pp. 43–61, DOI: https://doi.org/10.3221/IGF-ESIS.60.04.
[21] Jiang, C., Li, W., Ng, C.-T., Deng, M. (2024). Quasistatic component generation of group velocity mismatched guided waves in tubular structures for microdamage localization, Appl. Acoust., 217, pp. 109813, DOI: https://doi.org/10.1016/j.apacoust.2023.109813.
[22] Sadovský, Z., Kriváček, J., Ivančo, V., Ďuricová, A. (2012). Computational modelling of geometric imperfections and buckling strength of cold-formed steel, J. Constr. Steel Res., 78, pp. 1–7, DOI: https://doi.org/10.1016/j.jcsr.2012.06.005.
[23] Ibañez, C., Hernández-Figueirido, D., Piquer, A. (2021). Effect of steel tube thickness on the behaviour of CFST columns: Experimental tests and design assessment, Eng. Struct., 230, pp. 111687. DOI: https://doi.org/10.1016/j.engstruct.2020.111687.
[24] He, Z., Zhou, X. (2014). Strength design curves and an effective width formula for cold-formed steel columns with distortional buckling, Thin-Walled Struct., 79, pp. 62–70, DOI: https://doi.org/10.1016/j.tws.2014.02.004.
[25] Rath, B., Kiflu, F., Dereje, B., Garoma, S., Kebede, K., Gutema, E.M. (2022). Effect of different geometric factors of H-shaped steel section on bi-axially loaded fully encased composite column, J. Eng. Appl. Sci., 69(1), pp. 117, DOI: https://doi.org/10.1186/s44147-022-00169-2.